Fluctuation electron microscopy of Al-based metallic glasses: effects of minor alloying addition and structural relaxation on medium-range structural homogeneity

2007 J. Phys.: Condens. Matter 19 455211

(http://iopscience.iop.org/0953-8984/19/45/455211)

IOP PUBLISHING JOURNAL OF PHYSICS: CONDENSED MATTER

J. Phys.: Condens. Matter **19** (2007) 455211 (10pp) doi:10.1088/0953-8984/19/45/455211

Fluctuation electron microscopy of Al-based metallic glasses: effects of minor alloying addition and structural relaxation on medium-range structural homogeneity

J Wen[1], H W Yang[1], H Guo[1], B Wu[1], M L Sui[1], J Q Wang[1] and E Ma[2]

[1] Shenyang National Laboratory for Materials Science (SYNL), Institute of Metal Research, Chinese Academy of Sciences, Shenyang 110016, People's Republic of China
[2] Department of Materials Science and Engineering, The Johns Hopkins University, Baltimore, MD 21218, USA

E-mail: jqwang@imr.ac.cn and ema@jhu.edu

Received 4 August 2007, in final form 5 August 2007
Published 24 October 2007
Online at stacks.iop.org/JPhysCM/19/455211

Abstract

Al-based metallic glasses with relatively high glass-forming ability have been studied using fluctuation electron microscopy (FEM). These glasses exhibited well-defined glass transition and remained fully amorphous throughout the FEM experiments. Peaks were observed in the normalized intensity variance curves, evolving with sample composition and thermal history, while diffraction patterns remained identical. Specifically, minor alloying of Co into the $Al_{85}Ni_5Y_{10}$ glass improved its medium-range homogeneity. This is in accord with, and partly explains, the increase in the glass-forming ability. After annealing of $Al_{85}Ni_5Y_8Co_2$ below its glass transition temperature, FEM suggests structural homogenization or intensified medium-range fluctuations, depending on the annealing temperature. Such dissolution versus growth of quenched-in heterogeneity accompanying structural relaxation was not detectable using other techniques.

(Some figures in this article are in colour only in the electronic version)

1. Introduction

Al-based metallic glasses (MGs) with high specific strength have attracted much attention in recent years [1]. These MGs are interesting also because their crystallization behavior and mechanical properties have been observed to be highly sensitive to their chemical composition, as well as to the quenching condition or subsequent structural relaxation they have experienced [1–6]. The origin of such behavior is not well understood. One natural

proposal is that the 'structure' of these MGs changes easily with minor addition of alloying elements or with relaxation. But, without long-range order, the overall structure of all these MGs appears to be the same, i.e. simply amorphous. The short-range structure inside the glasses can be characterized statistically by two-body correlation functions which can be measured via diffraction measurements. Unfortunately, the x-ray or electron diffraction patterns, and the pair correlation functions derived thereof, are almost identical for these MGs. In other words, the short-range order (SRO) is not obviously different when only minor alloying or moderate relaxation is involved, and cannot account for the obvious differences observed in their properties (see below).

It is then possible that the structural differences lie in the 'medium range', i.e. beyond about the second nearest neighbor to a scale of the order of one nanometer. This is, however, a length scale difficult to probe using traditional structural characterization tools. The recent development of fluctuation electron microcopy (FEM) has brought some promise to this challenging problem [7–10]. FEM is sensitive to higher-order (three- and four-body) atomic correlations that persist well into the nanometer range [7–10]. FEM measures diffraction from nanoscale volumes using dark-field transmission electron microscopy (TEM) at a deliberately low image resolution. The image contrast comes from fluctuations in the scattering intensity. The strength of the fluctuations can be quantified using the statistical variance in the spatial image intensity distribution

$$V(k, Q) = \frac{\langle I^2(r, k, Q)\rangle}{\langle I(r, k, Q)\rangle^2} - 1 \tag{1}$$

where $I(r, k, Q)$ is the image intensity as a function of position r in the image, the scattering vector k, and the objective aperture size Q. $\langle\,\rangle$ denotes averaging over the image.

FEM was originally applied to examine medium-range order (MRO) in covalently bonded amorphous materials, e.g. Si and Ge [7, 11], and fruitful results were obtained for this type of disordered material (see [8] and the references therein). For MGs, only preliminary experimental data are available from the studies of Li *et al* [12] and Stratton *et al* [13]. The latter study was in fact on an Al-rich amorphous alloy, $Al_{92}Sm_8$. However, Al–Sm is not a good glass former, such that the as-quenched amorphous Al–Sm was found to contain a large number of quenched-in Al crystal nuclei that dominated medium-range features on the nanometer scale [13]. The amorphous Al–Sm alloy did not exhibit a glass transition in calorimetry studies except at very high scanning rates, and is not expected to be very stable under electron irradiation during TEM observations.

The study reported here was designed to address several questions. First, we selected melt-spun $Al_{85}Ni_5Y_{10}$, which is a metallic glass showing clear glass transition before crystallization. It is a fairly good glass former and thick ribbons up to 120 μm have been reported to be fully glassy [2]. This MG has a relatively high crystallization temperature and is stable for observations in TEM. We carried out preliminary FEM characterization, which showed that the normalized intensity variance $V(k)$ of this MG is different from that of the Al–Sm alloy. Second, minor alloying with 2 at.% Co replacing Y was reported to dramatically increase the glass forming ability (GFA) to the extent that 900 μm thick, fully glassy, ribbons could be obtained [2]. It is therefore a good example for studying the effect of minor alloying on the medium-range structure, to reveal possible structural origins for the large GFA difference. Third, relaxation upon annealing, annihilating excess free volume, affects mechanical properties while the amorphous structure remains unchanged [14]. $Al_{85}Ni_5Y_8Co_2$, as a strong glass former and one of the most stable Al-based MGs, is a good example to study the annealing effects. This sample was reported to remain fully amorphous after annealing below 240 °C for 30 min [15]. FEM for two annealing temperatures indicates

that $Al_{85}Ni_5Y_8Co_2$ exhibits obvious MRO changes accompanying structural relaxation upon annealing.

2. Experimental details

Master alloys with compositions of $Al_{85}Ni_5Y_{10}$ and $Al_{85}Ni_5Y_8Co_2$ (at.%) were prepared by arc melting pure elements together on a water cooled copper plate under a Ti-gettered, ultra-high purity argon atmosphere. They were re-melted several times to ensure homogeneity. Melt spun ribbons, about 40 μm thick and 4 mm wide, were produced using a Buhler single-roller melt spinner at a wheel speed of 35 m s^{-1}. The as-quenched samples were examined by x-ray diffraction (XRD) using a Rigaku D/max 2400 diffractometer with Cu Kα radiation. To observe the effect of relaxation at temperatures below the glass transition temperature (T_g), the as-quenched $Al_{85}Ni_5Y_8Co_2$ was annealed at 200 or 230 °C for 30 min. Isothermal and constant-heating-rate (0.67 K s^{-1}) DSC experiments were performed using a Perkin–Elmer differential scanning calorimeter (DSC 7) under a flowing Ar atmosphere.

TEM samples were thinned by electropolishing in an electrolyte of 20 vol% nitric acid and 80 vol% methanol at −35 °C. Ion milling was avoided because it could produce structural changes in the glass and hence artifacts in $V(k)$ [12]. Because the samples may structurally age with time [16], specimens for FEM experiments were all examined within 48 h of thinning. Conventional TEM characterization was performed on a FEI Tecnai G^2 F30 electron microscope and a JEOL JEM-2010(HR) transmission electron microscope.

Variable coherence FEM was carried out in the hollow-cone dark field (HCDF) mode on the FEI Tecnai G^2 F30 TEM at 200 kV with an objective aperture of approximately 1 nm^{-1} radius which produced an image resolution of about 6.1 Å (fixed Q in equation (1)). Each $V(k)$ curve represents the average of measurements from at least ten areas of the sample. The error bar represents one standard deviation from the mean. The total sample area measured for each curve was about 0.053 μm^2. The measured $V(k)$ will change with sample thickness [10], so a scripting based on the DigitalMicrograph (DM) software package was used to ensure the same electron transmittance for the areas selected, before the acquisition of each image series. In this study, only areas with 70% ± 2% transmittance were selected.

HCDF images were recorded on the center area with 512 × 512 pixels of a CCD-camera (Gatan 894) with a pixel size of 14 mm^2. A typical series consisted of 26 HCDF images with k varying from 0.24 to 0.94 $Å^{-1}$. The acquisition time was kept constant at 10 s for all images instead of keeping the average of counts per image constant. This allowed the use of a single dark current read-out for the entire dark current correction, speeding up the image acquisition for the whole series and reducing beam damage. The statistical error in $V(k)$ that scales as $1/I(k)$ was ignored here with sufficient electron counts per pixel [17]. The mean intensity for the 10 s exposure of the HC dark field images was about 2800 counts for the lowest k (0.24 $Å^{-1}$) and 500 counts for the highest k (0.94 $Å^{-1}$). After acquisition all the images were processed to recover the original electron intensity using a previously documented procedure [10].

3. Results

3.1. $Al_{85}Ni_5Y_{10}$ versus $Al_{85}Ni_5Y_8Co_2$

A good glass displays a T_g signal in the DSC curve at a relatively low heating rate, corresponding to the transition from the glass state to the supercooled liquid state. The DSC scans are shown in figure 1 for our as-quenched $Al_{85}Ni_5Y_{10}$ and $Al_{85}Ni_5Y_8Co_2$ ribbons. Upon heating, a clearly resolvable endothermic signal corresponding to glass transition, with its onset

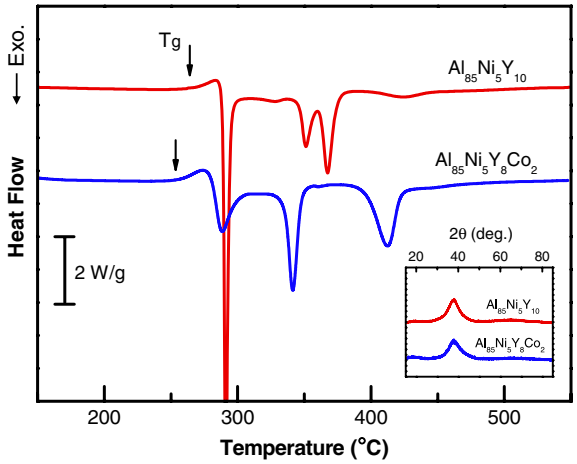

Figure 1. DSC traces of $Al_{85}Ni_5Y_{10}$ and $Al_{85}Ni_5Y_8Co_2$ MGs at a constant heating rate of 0.67 K s^{-1}. Both samples show obvious T_g. The inset is the XRD patterns for these two samples.

marked as T_g in the figure, was observed for both glasses at slightly different temperatures (265 °C for $Al_{85}Ni_5Y_{10}$ and 254 °C for $Al_{85}Ni_5Y_8Co_2$). Each glass exhibited three exothermic events due to crystallization. The first crystallization event happened at almost the same temperature, but the peak shape was different for the two MGs. The two subsequent exothermic peaks, on the other hand, were at very different positions. These behaviors were reported before [2], and our focus here is to examine if the two as-quenched MGs possess any difference in their glass structure.

The corresponding XRD patterns of these two MGs, shown in the inset in figure 1, are consistent with their amorphous state, but before and after the Co addition the XRD patterns look almost identical. As remarked in section 1, diffraction patterns (and the two-body pair correlation functions) do not offer useful clues as to why the very similar compositions show obviously different GFA and DSC curves. Electron diffraction patterns also confirm the XRD results (see figures 2(b) and (e)).

Figures 2(c) and (f) compare their high-resolution TEM (HRTEM) images. The typical maze patterns in the HRTEM images further confirm the fully amorphous nature, but once again there is no discernable difference between the two MGs.

The annular average of the typical electron diffraction patterns in figures 2(b) and (e) for the Co-free and Co-bearing samples are compared in figure 3(a). The differences in the electron diffraction spectra are subtle. This is consistent with the behavior in the XRD patterns reported above.

The search finally found some differences between the two MGs, in the speckle intensities and distributions in the HCDF images. The example in figures 2(a) and (d) compares HCDF images acquired at 0.44 $Å^{-1}$. They are displayed on the same intensity scale (also true for other HCDF images to be discussed below). $Al_{85}Ni_5Y_{10}$ apparently has greater intensity fluctuation than $Al_{85}Ni_5Y_8Co_2$. The normalized intensity variance curves $V(k)$, figure 3(b), quantify this difference. Both the $V(k)$ curves for the Co-free and Co-bearing samples have a main peak at about 0.43 $Å^{-1}$ and a weak peak at 0.68 $Å^{-1}$, but there is an obvious reduction in the height of the $V(k)$ peaks after adding Co. The addition of Co apparently did not change the MRO type, as the peak positions did not move, while the change in peak amplitude suggests that the as-quenched $Al_{85}Ni_5Y_8Co_2$ is more structurally homogeneous in the medium range than the

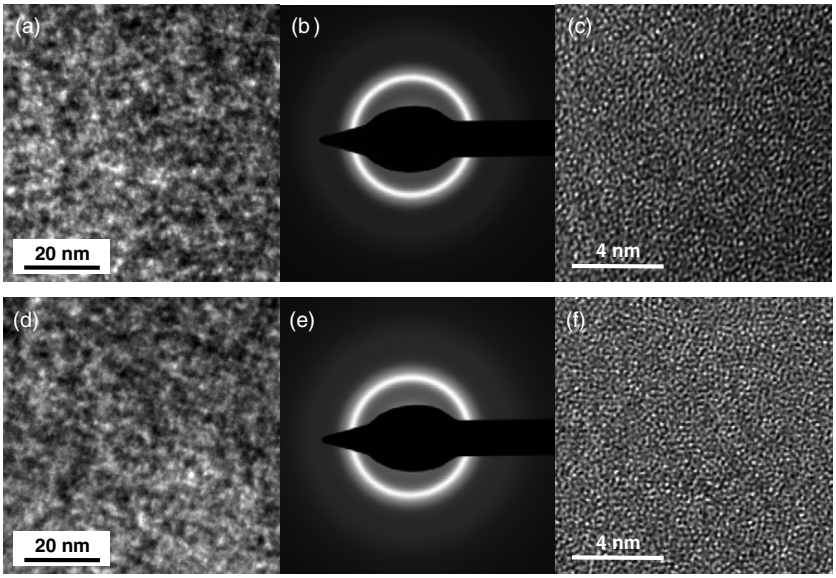

Figure 2. (a) Hollow-cone dark field (HCDF) image of $Al_{85}Ni_5Y_{10}$, (b) its corresponding electron diffraction pattern and (c) HRTEM micrograph; (d)–(f) are the counterparts for $Al_{85}Ni_5Y_8Co_2$. The HCDF images, displayed on the same intensity scale, were acquired at 0.44 $Å^{-1}$.

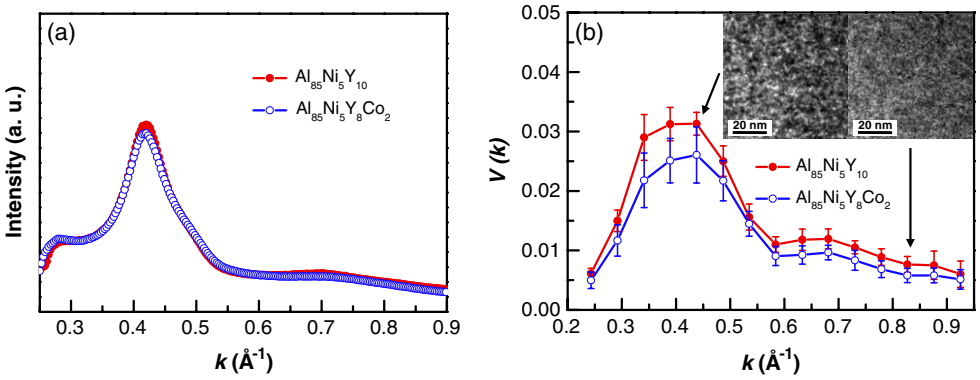

Figure 3. Electron diffraction intensity and normalized variance data for $Al_{85}Ni_5Y_{10}$ and $Al_{85}Ni_5Y_8Co_2$ MGs. The insets in (b) compare the HCDF images for $Al_{85}Ni_5Y_{10}$ at two different k values (0.44 $Å^{-1}$ versus 0.83 $Å^{-1}$).

$Al_{85}Ni_5Y_{10}$ glass prepared under similar conditions. This observed change in medium-range structural fluctuation will be discussed in section 4.

3.2. Annealing of the $Al_{85}Ni_5Y_8Co_2$ MG

To study the annealing effects on the glass structure, we chose $Al_{85}Ni_5Y_8Co_2$ because this multi-component alloy is more stable than the $Al_{85}Ni_5Y_{10}$ ternary glass [2]. The annealing was carried out isothermally at 200 °C and 230 °C for 30 min, respectively, for the as-quenched $Al_{85}Ni_5Y_8Co_2$. After annealing, the constant-heating-rate DSC scans are compared with the as-quenched sample, figure 4. The broad hump before glass transition, which was due to

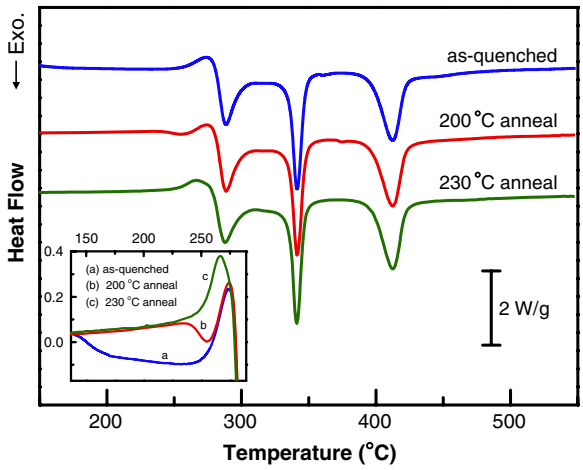

Figure 4. DSC curves of the as-quenched and annealed $Al_{85}Ni_5Y_8Co_2$ samples. Annealing below T_g gradually removes the structural relaxation signal (see the enlarged view in the inset), without changing the crystallization behavior: inset (a) as-quenched; (b) annealed at 200 °C for 30 min; (c) annealed at 230 °C for 30 min.

structural relaxation, disappeared mostly for the 200 °C-annealed sample, and completely for the 230 °C-annealed sample (see the enlarged view in the inset of figure 4). Such re-heating DSC experiments provided the indication that the isothermal annealing at 200 °C completed the majority of the structural relaxation of the as-quenched glass, whereas the 230 °C isothermal annealing corresponded to a constant-heating-rate scan all the way to T_g (see discussion below). The thermally induced structural relaxation is consistent with the notion that the free volume retained in the glass during quenching from the melt was gradually eliminated with increasing temperature. Compared to the as-quenched sample, the three crystallization peaks remain unchanged for the annealed samples, indicating that crystallization did not commence during the annealing.

Figure 5 shows the HCDF images acquired at 0.44 $Å^{-1}$, electron diffraction patterns and HRTEM micrographs for the as-quenched and the annealed $Al_{85}Ni_5Y_8Co_2$ samples. The typical maze patterns in the HRTEM images confirm the fully amorphous nature after annealing. From these images one cannot tell whether there is a change in local order, before and after annealing. Although the 230 °C annealed sample has stronger intensity variation than each of the other two samples, speckles in the HCDF images were still distributed homogeneously and no distinguishable bright regions were found to develop, which is consistent with the small-angle x-ray scattering (SAXS) experiments reported before. The samples remained fully amorphous and uniform after annealing for 30 min at temperatures below 240 °C [15].

The electron diffraction and normalized variance curves $V(k, Q)$ for the as-quenched and annealed samples are given in figure 6. The diffraction intensity curves remained identical, as shown in figure 6(a). However, the normalized variance plots in figure 6(b) show obvious differences in $V(k)$ intensities, but not their positions. This is indicative of the same MRO type, but different degrees of structural homogeneity. The suppression of the height of the variance peaks suggests that annealing at 200 °C rendered the sample more structurally homogeneous than the as-quenched sample. Annealing at the higher temperature (230 °C), on the other hand, increased the magnitude of the $V(k)$ peaks, in such a pronounced way that it became even

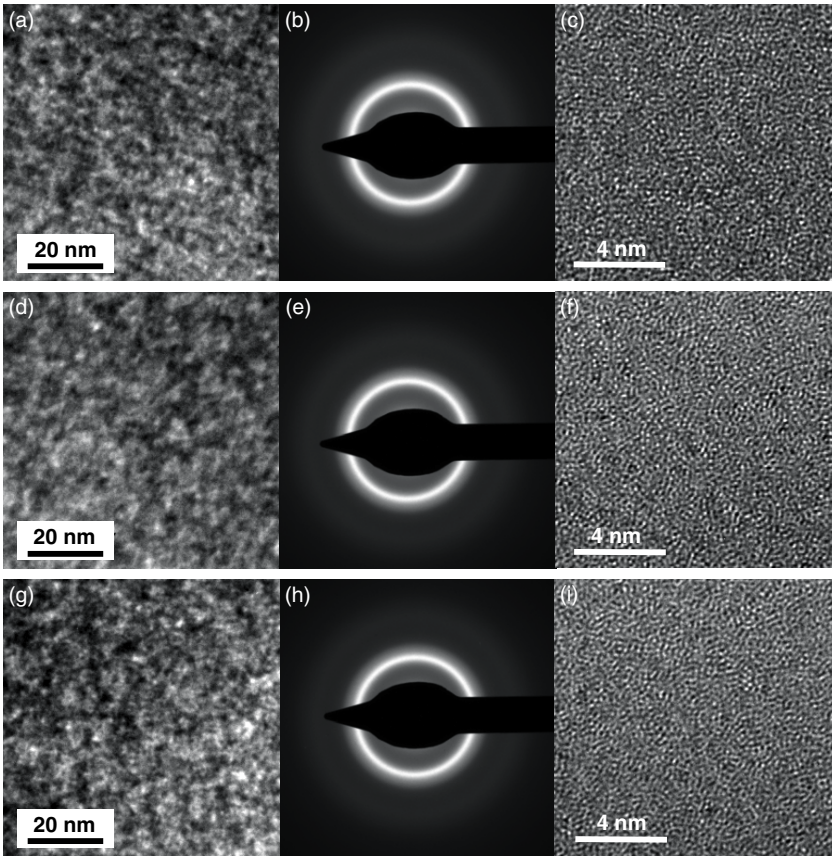

Figure 5. From left to right, typical hollow-cone dark field (HCDF) images, electron diffraction patterns and HRTEM micrographs for as-quenched and annealed $Al_{85}Ni_5Y_8Co_2$: (a)–(c) as-quenched; (d)–(f) annealed at 200 °C for 30 min; (g)–(i) annealed at 230 °C for 30 min. The HCDF images were acquired at the $V(k)$ peak position (∼0.44 $Å^{-1}$) and displayed on the same intensity scale.

greater than the as-quenched sample. Some medium-range structural fluctuation has developed in the 230 °C-annealed sample, even though other conventional techniques (such as XRD, DSC, and HRTEM) failed to detect these differences.

4. Discussion

There are several issues that need to be explained and discussed. Firstly, one may notice that the image resolution used was higher than those used by others [8]. This results in the relatively low resolution in the $V(k)$ plot. It also renders our $V(k)$ measurements more sensitive to features in the near-medium range, i.e. subnanometer to nanometer sizes [18]. Due to limitations with our instrument and the available objective aperture, we have not yet varied the resolution in this first set of experiments to reach the optimum condition for measuring MRO. However, it is likely that the MRO developed in monolithic, truly amorphous MGs would have dimensions only in the range of $<\sim$1 nm, smaller than those paracrystals found in amorphous semiconductors such as Si [11]. Indeed, in these latter non-metallic glasses, strong bright regions can be

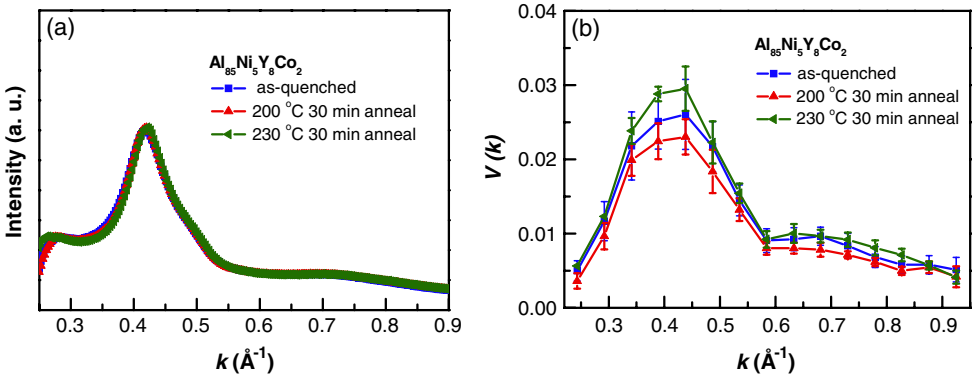

Figure 6. Electron diffraction intensity and normalized variance curves for as-quenched and annealed $Al_{85}Ni_5Y_8Co_2$ samples. The diffraction spectra in (a) are almost identical, whereas the changes in normalized variance (b) are obvious. The suppression or promotion of normalized variance upon annealing at different temperatures depends on the dissolution or growth of quenched-in heterogeneity.

found in HCDF images [19, 20]. The speckles in our HCDF images, in comparison, distribute homogeneously without clustering into bright regions. This suggests that the MGs are of greater structural homogeneity in the sense that they may have shorter MRO scales than amorphous semiconductors.

Second, we need to justify the claim that the $V(k)$ changes observed in figures 3 and 6 suggest structural variability in the medium range. The key supporting argument is that in figures 3 and 6 the FEM $V(k)$ showed obvious changes when diffraction intensity did not. In general, the diffracted intensity $I(k)$ is sensitive only to the two-body function, whereas the variance $V(k)$ is more sensitive to higher-order functions. Because $V(k)$ contains contributions from two-body, three-body, and four-body correlations, for a $V(k)$ peak that broadly tracks $I(k)$ the two-body correlation may be a major contributor [18]. Our $V(k)$ peaks do resemble $I(k)$, in terms of their shapes and positions. However, figures 3 and 6 demonstrate that when $I(k)$ was not changing (statistically the two-body correlation was presumably unchanged as well), $V(k)$ appeared to have been altered, due to contributions obviously not from the two-body functions. This difference in behavior between $V(k)$ and $I(k)$ indicates that the normalized variance and the electron diffraction are not simply redundant signals [18]. Additional information is provided by the variance $V(k)$ regarding higher-order correlations and medium-range structural fluctuation.

The third point, which should be emphasized, is that the increased medium-range homogeneity observed in the Co-containing MG is consistent with its higher GFA. The higher GFA implies that the supercooled melt is more viscous and allows less fluctuation towards crystallization, making it easier to retain a truly amorphous structure when cooled to below the glass transition temperature. The resulting glass state is thus likely to be more homogeneous. At a worse glass-forming composition, there would be higher driving forces and faster kinetics in the supercooled liquid to allow more fluctuation and heterogeneity, rendering a higher chance for the emergence of well-ordered local regions (regions with strong MRO). The suppression of crystallization is hence more difficult during the rapid cooling process. In this case, when a glass is obtained the heterogeneity retained inside the amorphous structure is likely to be more pronounced. What exactly Co does to change the liquid structure/behavior remains unknown, however.

Finally, there is a fourth issue, regarding how the annealing affected medium-range structural homogeneity. Moderate relaxation at 200 °C appeared to have improved homogeneity in the glass. Such an observation was made before in other glasses [11, 19]. One could imagine that in the glass there are always some quenched-in heterogeneities including subcritical embryos of crystals. At a low annealing temperature well below T_g, the expected population of sub-critical nuclei would be low. The glass state does not allow much structural fluctuations. Some of the ordered regions quenched-in would in fact dissolve [11, 19]. Other heterogeneities such as free volume would also be annihilated during relaxation. These effects explain why the glass becomes apparently more homogeneous. In contrast, the higher annealing temperature (230 °C) was getting rather close to T_g, so the long hold (30 min) could bring in some behavior of a supercooled liquid, in which fluctuation is more pronounced. A distribution of subcritical and some supercritical nuclei is likely to build up. Indeed, reheating the 230 °C annealed sample in the DSC (figure 4) showed that all the relaxation signals exhibited by the as-quenched sample before T_g were no longer present (see inset of figure 4), making the T_g dip more obvious. This suggests that the material has been annealed to an extent equivalent to reaching T_g. When quenched back to room temperature, the glass remained amorphous, figures 5(g)–(i), but the structural fluctuation in the medium range became more pronounced, as the glass had the chance for a thermal excursion to a state very near or even slightly above T_g, where the glass could (partially) turn into supercooled liquid and become much less viscous. As for the first crystallization peak during DSC heating of the annealed samples, for both cases it would depend on the eventual structure of the sample upon reaching the crystallization temperature in the DSC (i.e. the glass after being heated well into the supercooled liquid region). As a result, the prior annealing at the lower temperatures is not expected to cause obvious changes to the subsequent crystallization peaks in figure 4.

Our annealing results can also explain the findings in [4] and [5], where the primary crystallization of Al, observed during continuous heating or after annealing above the glass-transition temperature, did not occur during isothermal annealing below T_g. Instead, an unknown metastable phase was formed conjointly with α-Al via a eutectic-like mechanism. As we discussed above, low temperature (200 °C) annealing makes the sample more homogeneous, with the dissolution of quenched-in heterogeneities. Primary Al precipitation as the first crystallization event may thus be suppressed.

5. Summary remarks

Fluctuation electron microscopy suggests medium-range fluctuations in fully amorphous $Al_{85}Ni_5Y_{10}$ and $Al_{85}Ni_5Y_8Co_2$ MGs, in the absence of a high population of quenched-in, pre-existing nanocrystals. A minor alloying with 2 at.% Co replacing Y in $Al_{85}Ni_5Y_{10}$ reduces the peak height of the $V(k)$ curve, suggesting a more uniform glass structure, which is expected for a glass with higher glass-forming ability. Annealing at different temperatures of the $Al_{85}Ni_5Y_8Co_2$ MG resulted in varying amplitudes of $V(k)$ peaks, suggesting that structural homogenization or development of heterogeneity can happen in the course of structural relaxation, depending on how close the glass has come to the supercooled liquid state. Note that all the effects of alloying or annealing revealed here via FEM had escaped detection when other techniques were used.

It should be noted, however, that more in-depth research is required to resolve the various sources of correlations present in glasses dominated by metallic bonding. Al-based MGs are solute-lean, so that the solute-centered quasi-equivalent clusters (with only solvent Al atoms surrounding the center solute) should be the structural motifs [21]. The varying degrees of organization of these clusters into super-clusters $\sim$1 nm in size, via sharing and ordering

schemes towards dense packing [21], may be a source for the variations in the medium-range structure. Also, due to the high Al content in the alloy, local Al-like clusters and quenched-in nuclei are possible [13]. Even subnanometer-scale entities, below the critical size of crystal nuclei observed in previous studies [13], may lead to near medium-range structural fluctuations visible in the FEM. These details aside, FEM is apparently useful as a tool to globally sense the structural heterogeneities in the medium range, helpful for studying the effects of sample composition and thermal history.

Acknowledgments

This work was supported by the National Natural Science Foundation of China (Grant Nos. 50471076, 50323009 and 50671104). The authors were part of the MANS research team, supported in part by the Chinese Academy of Sciences.

References

[1] Inoue A 1998 *Prog. Mater. Sci.* **43** 365–520
[2] Inoue A, Matsumoto N and Masumoto T 1990 *Mater. Trans., JIM* **31** 493–500
[3] Yang H W, Dong P, Wang J Q and Li Y 2007 *Mater. Sci. Eng.* A **449–451** 273–6
[4] Louzguine D V and Inoue A 2001 *Appl. Phys. Lett.* **78** 3061–3
[5] Louzguine D V and Inoue A 2002 *Mater. Lett.* **54** 75–80
[6] Kelton K F 2007 private communications
[7] Treacy M M J and Gibson J M 1996 *Acta Crystallogr.* A **52** 212–20
[8] Treacy M M J, Gibson J M, Fan L, Paterson D J and McNulty I 2005 *Rep. Prog. Phys.* **68** 2899–944
[9] Gibson J M, Treacy M M J and Voyles P M 2000 *Ultramicroscopy* **83** 169–78
[10] Voyles P M 2000 *PhD Dissertation* University of Illinois at Urbana-Champaign
[11] Treacy M M J, Gibson J M and Keblinski P J 1998 *J. Non-Cryst. Solids* **231** 99–110
[12] Li J, Gu X and Hufnagel T C 2003 *Microsc. Microanal.* **9** 509–15
[13] Stratton W G, Hamann J, Perepezko J H, Voyles P M, Mao X and Khare S V 2005 *Appl. Phys. Lett.* **86** 141910
[14] Jiang W H, Pinkerton F E and Atzmon M 2005 *Acta Mater.* **53** 3469–77
[15] Yang H W, Wang J Q and Ohnurna M 2006 *J. Mater. Res.* **21** 2215–23
[16] Stratton W G, Hamann J, Perepezko J H and Voyles P M 2004 Amorphous and nanocrystalline metals *MRS Symp. Proc.* vol 806 (MM9.4.1)
[17] Voyles P M and Muller D A 2002 *Ultramicroscopy* **93** 147–59
[18] Treacy M M J 2007 *Ultramicroscopy* **107** 166–71
[19] Gibson J M and Treacy M M J 1997 *Phys. Rev. Lett.* **78** 1074–7
[20] Kwon M H, Lee B S, Bogle S N, Nittala L N, Bishop S G, Abelson J R, Raoux S, Cheong B K and Kim K B 2007 *Appl. Phys. Lett.* **90** 021923
[21] Sheng H W, Luo W K, Alamgir F M, Bai J M and Ma E 2006 *Nature* **439** 419–25